

Pathomic Fusion: An Integrated Framework for Fusing Histopathology and Genomic Features for Cancer Diagnosis and Prognosis

Richard J. Chen, Ming Y. Lu, Jingwen Wang, Drew F. K. Williamson, Scott J. Rodig,
Neal I. Lindeman and Faisal Mahmood*

Abstract—Cancer diagnosis, prognosis and therapeutic response predictions are based on morphological information from histology slides and molecular profiles from genomic data. However, most deep learning-based objective outcome prediction and grading paradigms are based on histology or genomics alone and do not make use of the complimentary information in an intuitive manner. In this work, we propose *Pathomic Fusion*, a strategy for end-to-end multimodal fusion of histology image and genomic (mutations, CNV, mRNAseq) features for survival outcome prediction and patient stratification, where histologic features are also learned via graph convolutional networks (GCNs). Our approach models pairwise feature interactions across modalities by taking the Kronecker product of gated feature representations, and controls the expressiveness of each representation via a gating-based attention mechanism. The proposed framework is able to model pairwise interactions across features in different modalities and control their relative importance. We validate our approach using glioma datasets from the Cancer Genome Atlas (TCGA), which contains paired whole-slide image, genotype, and transcriptome data with ground truth survival and histologic grade labels. Based on a rigorous 15-fold cross validation, our results demonstrate that the proposed multimodal fusion paradigm improves prognostic determinations from grading and molecular subtyping as well as unimodal deep networks trained on histology and genomic data alone. The proposed method establishes insight and theory on how to train deep networks on multimodal biomedical data in an intuitive manner, which will be useful for other problems in medicine that seek to combine heterogeneous data streams for understanding diseases and predicting response and resistance to treatment. Code and trained models are made available at: <https://github.com/mahmoodlab/PathomicFusion>.

Index Terms—Multimodal Learning, Graph Convolutional Networks, Survival Analysis

I. INTRODUCTION

Cancer diagnosis, prognosis and therapeutic response prediction is usually accomplished using heterogeneous data sources including histology slides, molecular profiles, as well as clinical data such as the patient’s age and comorbidities. Histology-based subjective and qualitative analysis of the tumor microenvironment coupled with quantitative examination of genomic assays is the standard-of-care for most cancers in

modern clinical settings [1]–[4]. As the field of anatomic pathology migrates from glass slides to digitized whole slide images, there is a critical opportunity for development of algorithmic approaches for joint image-omic assays that make use of phenotypic and genotypic information in an integrative manner.

The tumor microenvironment is a complex milieu of cells that is not limited to only cancer cells, as it also contains immune, stromal, and healthy cells. Though histologic analysis of tissue provides important spatial and morphological information of the tumor microenvironment, the qualitative inspection by human pathologists has been shown to suffer from large inter- and intraobserver variability [5]. Moreover, subjective interpretation of histology slides does not make use of the rich phenotypic information that has shown to have prognostic relevance [6]. Genomic analysis of tissue biopsies can provide quantitative information on genomic expression and alterations, but cannot precisely isolate tumor-induced genotypic measures and changes from those of non-tumor entities such as normal cells. Though modern sequencing technologies such as single cell sequencing and spatial transcriptomics are being developed to spatially-resolve genomic information, these technologies currently lack clinical penetration.

Oncologists often rely on both the qualitative information from histology and quantitative information from genomic data to predict clinical outcomes [7], however, most histology analysis paradigms do not incorporate genomic information. Moreover, such methods often do not explicitly incorporate information from the spatial organization and community structure of cells, which have known diagnostic and prognostic relevance [6], [8]–[10]. Fusing morphological information from histology and molecular information from genomics provides an exciting possibility to better quantify the tumor microenvironment and harness deep learning-based for the development of image-omic assays for early diagnosis, prognosis, patient stratification, survival, therapeutic response and resistance prediction.

Contributions: The contributions of this paper are highlighted as follows:

- **Novel Multimodal Fusion Strategy:** We propose *Pathomic Fusion*, a novel framework for multimodal fusion of histology image, cell graph, and genomic modalities (Fig. 1). Our proposed method models pairwise feature interactions across modalities by taking the Kronecker product of gated feature representations, and controls the

(Corresponding Author: Faisal Mahmood faisal Mahmood@bwh.harvard.edu). All authors are with the Department of Pathology, Brigham and Women’s Hospital, Harvard Medical School, Boston, MA. R.C. M.L. and F.M. also with the Broad Institute of Harvard and MIT and the at Dana-Farber Cancer Institute, Boston, MA. R.C. is also with the Department of Biomedical Informatics, Harvard Medical School, Boston, MA. email: richardchen@g.harvard.edu; [m1u16,jwang111,dwilliamson,srodig,nlindeman}@bwh.harvard.edu](mailto:{m1u16,jwang111,dwilliamson,srodig,nlindeman}@bwh.harvard.edu)

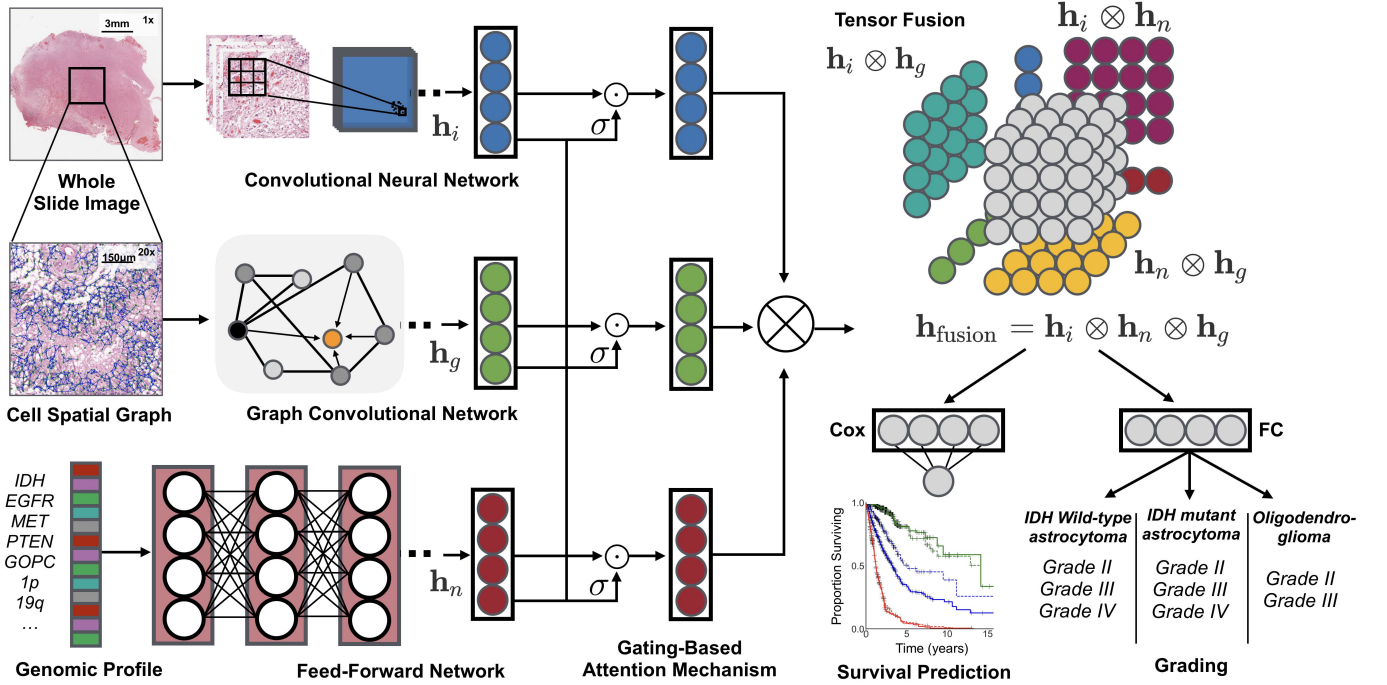


Fig. 1: *Pathomic Fusion*: An integrated framework for multimodal fusion of histology image, cell graph and genomic features for survival outcome prediction and cancer grade classification. Histology features are being extracted in two different approaches using CNNs and GCNs. Unimodal networks for the respective image, graph, and genomic features are first trained individually for the corresponding supervised learning task, and then used as feature extractors for multimodal fusion. Multimodal fusion is performed by applying an gating-based attention mechanism to first control the expressiveness of each modality, followed by the Kronecker product to model pairwise feature interactions across modalities.

expressiveness of each representation using a gating-based attention mechanism.

- **GCNs for Cancer Outcome Prediction:** We present a novel approach for learning morphometric cell graph features in histopathology tissue using graph convolutional networks (Fig. 2), and present the application of GCNs for cancer survival outcome prediction from histology.
- **Objective Image-Omic Outcome Prediction and Quantitative Study:** Using a rigorous 15-fold cross-validation-based analysis, we demonstrate that our proposed multimodal fusion of histology and genomic features outperforms subjective prognostic determinations based on the WHO grading paradigm for diffuse gliomas. Moreover, we show that our image-omic paradigm surpasses current objective-based histology approaches that use CNNs for supervised learning, as well as the current state-of-the-art in using concatenation to combine histology and genomics.

II. RELATED WORK

Survival Analysis for Cancer Outcome Prediction: Cancer prognosis via survival outcome prediction is a standard method used for biomarker discovery, stratification of patients into distinct treatment groups, and therapeutic response prediction [11]. With the availability of high-throughput data from next-generation sequencing, Statistical survival models have become one of the mainstay approaches for performing retrospective studies in patient cohorts with known cancer outcomes, with common covariates including copy number variation (CNV), mutation status, and RNA sequencing (RNAseq) expression

[11], [12]. Recent work has incorporated deep learning into survival analysis, in which the covariates for a Cox model are learned using a series of fully connected layers. Yousefi *et al.* [13] proposed using stacked denoising autoencoders to learn a low dimension representation of RNAseq data for survival analysis, and in a follow-up work [13], they used Feedforward Networks to examine the relationship between gene signatures and survival outcomes. Huang *et al.* [14] proposed using weighted gene-expression network analysis as another approach for dimensionality reduction and learning eigen-features from RNAseq and micro-RNA data for survival analysis in TCGA. However, these approaches do not incorporate the wealth of multimodal information from heterogeneous data sources including diagnostic slides, which may capture the inherent phenotypic tumor heterogeneity that has known prognostic value.

Multimodal Deep Learning: Multimodal fusion via deep learning has emerged as an interdisciplinary field that seeks to correlate and combine disparate heterogeneous data modalities to solve difficult prediction tasks in areas such as visual perception, human-computer interaction, and biomedical informatics [15]. Depending on the problem, approaches for multimodal fusion range from fusion of multiview data of the same modality, such as the collection of RGB, depth and infrared measurements for visual scene understanding, to the fusion of heterogeneous data modalities, such as integrating chest X-rays, textual clinical notes, and longitudinal measurements for intensive care monitoring [16]. In the natural language

processing community, Kim *et al.* [17] proposed a low-rank feature fusion approach via the Hadamard product for visual question answering, often referred to as bilinear pooling. Zadeh *et al.* [18] studied feature fusion via the Kronecker product for sentiment analysis in audio-visual speech recognition.

Multimodal Fusion of Histology and Genomics: Though many multimodal fusion strategies have been proposed to address the unique challenges in computer vision and natural language processing, strategies for fusing data in the biomedical domain (e.g. histology images, molecular profiles) are relatively unexplored. In cancer genomics, most works have focused on establishing correspondences between histology tissue and genomics [19]–[22]. For solving supervised learning tasks, previous works have generally relied on the ensembling of extracted feature embeddings from separately trained deep networks (termed late fusion) [14], [23], [24]. Morbadersany *et al.* [23] proposed a strategy for combining histology image features with a single gene mutation and chromosome codeletion for survival outcome prediction via vector concatenation. Cheerla *et al.* [25] developed an unsupervised multimodal encoder network for integrating histology image and genomic modalities via concatenation that is resilient to missing data. Shao *et al.* [26] proposed an ordinal multi-modal feature selection approach that identifies important features from both pathological images and multi-modal genomic data, but relies on handcrafted features from morphometric cell graph features in histology images. Beyond late fusion, there is limited work in deep learning-based multimodal learning approaches that combine histology and genomic data.

Graph-based Histology Analysis: Though CNNs have achieved remarkable performance in histology image classification and feature representation, graph-based histology analysis has become a promising alternative that rivals many competitive benchmarks. The motivation for interpreting histology images as a graph of cell features (cell graph) is that these morphometric features are more easily computed, and explicitly capture cell-to-cell interactions and their spatial organization with respect to the tissue. Prior to deep learning, previous works in learning morphological features from histology images have relied on manually constructed graphs and computing predefined statistics. Doyle *et al.* [27] was the first work to approach Gleason score grading in prostate cancer using Voronoi and Delauney tessellations. Shao *et al.* [26] presented an interesting approach for feature fusion of graph and molecular profile features, with graph features constructed manually and fused via vector concatenation similar to Huang *et al.* [14]. Motivated by the success of representation learning in graphs using deep networks [28]–[31], Anand *et al.* [9], Zhou *et al.*, [32] and Wang *et al.* [10] have used graph convolutional networks for breast, colon and prostate cancer histology classification respectively. Currently, however, there have been no deep learning based-approaches that have used graph convolutional networks for survival outcome prediction.

III. METHODS

Given paired histology and genomic data with known cancer outcomes, our objective is to learn a robust multimodal

representation from both modalities that would outperform unimodal representations in supervised learning. Previous works have only relied on CNNs for extracting features from histology images, and late fusion for integrating image features from CNNs with genomic features. In this section, we present our novel approach for integrating histology and genomic data, *Pathomic Fusion*, which fuses histology image, cell graph, and genomic features into a multimodal tensor that explicitly models bimodal and trimodal interactions from each modality. In *Pathomic Fusion*, histology features are extracted as two different views: image-based features using Convolutional Neural Networks (CNNs), and graph-based features using Graph Convolutional Networks (GCNs). Both networks would extract similar morphological features, however, cell graphs from histology images are a more explicit feature representation that directly model cell-to-cell interactions and cell community structure. Following the construction of unimodal features, we propose a gating-based attention mechanism that controls the expressiveness of each feature before constructing the multimodal tensor. The objective of the multimodal tensor is to capture the space of all possible interactions between features across all modalities, with the gating-based attention mechanism used to regularize unimportant features. In subsections A-C, we describe our approach for representation learning in each modality, with subsections D describing our multimodal learning paradigm. Additional implementation and training details are found in Appendix B.

A. Learning Patient Outcomes from H&E Histology Tissue Images using Convolutional Neural Networks

Anatomic pathology has the ability to reveal the inherent phenotypic intratumoral heterogeneity of cancer, and has been an important tool in cancer prognosis for the past century [33]–[36]. Tumor microenvironment features such as high cellularity and microvascular proliferation have been extensively linked to tumor suppressor deficiency genes and angiogenesis, and recognized to have clinical implications in the recurrence and proliferation of cancer [37]. To capture these features, we train a Convolutional Neural Network (CNN) on 512×512 random image crops from 1024×1024 regions-of-interest (ROIs) at $20\times$ magnification as representative regions of cancer pathology. We use 512×512 random image crops to increase the number of training images in our dataset, and to strike a balance between using the entire 1024×1024 image which would prevent training with larger batch sizes, and standard 256×256 image crops that might leave out important histology tissue patterns and spatial structures. To use the entire image for survival outcome prediction, we decompose the image into 16 overlapping 512×512 patches, and then average the hazards. The network architecture of our CNN is VGG19 with batch normalization, which we finetuned using pre-existing weights trained on ImageNet. We extract a $\mathbf{h}_i \in \mathcal{R}^{32 \times 1}$ embedding from the last hidden layer of our Histology CNN, which we use as input into *Pathomic Fusion*. This network is supervised by the Cox partial likelihood loss for survival outcome prediction, and cross entropy loss for grade classification (Appendix A).

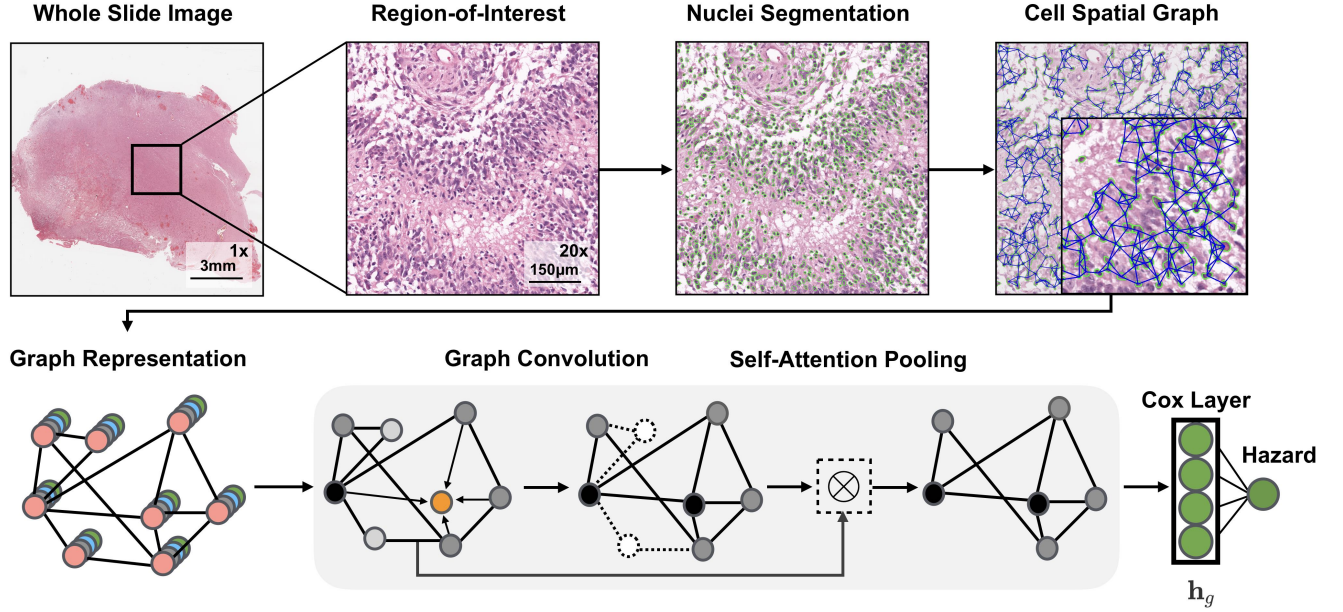


Fig. 2: Graph Convolutional Network for learning morphometric cell features from histology images. We represent cells in histology tissue as nodes in a graph, where cells are isolated using a deep learning-based nuclei segmentation algorithm and the connections between cells are made using KNN. Features for each cell are initialized using handcrafted features as well as deep features learned using contrastive predictive coding. The aggregate and combine functions are adopted from the GraphSAGE architecture, with the node masking and hierarchical pooling strategy adopted from SAGPool.

B. Learning Morphometric Cell and Graph Features using Graph Convolutional Networks

The spatial heterogeneity of cells in histopathology has potential in informing the invasion and progression of cancer and in bioinformatic tasks of interest such as cancer subtyping, biomarker discovery and survival outcome prediction [33], [38]. Unlike image-based feature representation of histology tissue using CNNs, cell graph representations explicitly capture only pre-selected features of cells, which can be scaled to cover larger regions of histology tissue.

Let $G = (V, E)$ denote a graph with nodes V and edges E . We define $X \in \mathcal{R}^{N \times F}$ as a feature matrix of N nodes in V with F -dimensional features, and $A \in \mathcal{R}^{N \times N}$ as the adjacency matrix that holds the graph topology. To construct graphs that would capture the tumor microenvironment (Fig 2), on the same 1024×1024 ROI used as input to our CNN, we 1): perform semantic segmentation to detect and spatially localize cells in a histopathology region-of-interest to define our set of nodes V , 2): use K-Nearest Neighbors to find connections between adjacent cells to define our set of edges E , 3): calculate handcrafted and deep features for each cell that would define our feature matrix X , and 4): use graph convolutional networks to learn a robust representation of our entire graph for survival outcome prediction.

Nuclei Segmentation: Accurate nuclei segmentation is important in defining abnormal cell features such as nuclear atypia, abundant tumor cellularity, and other features that would be indicative of cancer progression [39]–[42]. Previous works rely on conventional fully convolutional networks that minimize a pixel-wise loss [43], which can cause the network to segment multiple nuclei as one, leading to inaccurate feature extraction of nuclei shape and community structure. To overcome this

issue, we use conditional generative adversarial networks (cGAN) to learn an appropriate loss function for semantic segmentation, which circumvents manually engineered loss functions [44]–[46]. As described in our previous work [44], the conditional GAN framework consists of two networks (a generator G and a discriminator D) that compete against each other in a min-max game to respectively minimize and maximize the objective $\min_G \max_D \mathcal{L}(G, D)$. Specifically, G is a segmentation network that learns to translate histology tissue images n into realistic segmentation masks m , and D is a binary classification network that aims to distinguish real and predicted pairs of tissue ((n, m) vs. $(n, S(n))$). Our generator is supervised with a \mathcal{L}_1 loss and adversarial loss function, in which the adversarial loss penalizes the generator for producing segmentation masks that are unrealistic.

$$\begin{aligned} \mathcal{L}_{\text{GAN}}(S, D_M) = & \mathbb{E}_{m, n \sim p_{\text{data}}(m, n)} [\log D_M(m, n)] \\ & + \mathbb{E}_{n \sim p_{\text{data}}(n)} [\log (1 - D_M(m, S(n)))] \end{aligned}$$

Cell Graph Construction: From our segmented nuclei, we use the K -Nearest Neighbors (KNN) algorithm from the Fast Library for Approximate Nearest Neighbours (FLANN) library to construct the edge set and adjacency matrix of our graph [47] (Fig 2). We hypothesize that adjacent cells will have the most significant cell-cell interactions and limit the adjacency matrix to K nearest neighbours. In our investigations, we used $K = 5$ to detect community structure and model cellular interactions. Using KNN, our adjacency matrix A is defined as:

$$A_{ij} = \begin{cases} 1 & \text{if } j \in \text{KNN}(i) \text{ and } D(i, j) < d \\ 0 & \text{otherwise} \end{cases}$$

Manual Cell Feature Extraction: For each nucleus, we computed statistics such as roundness, area, color intensity,

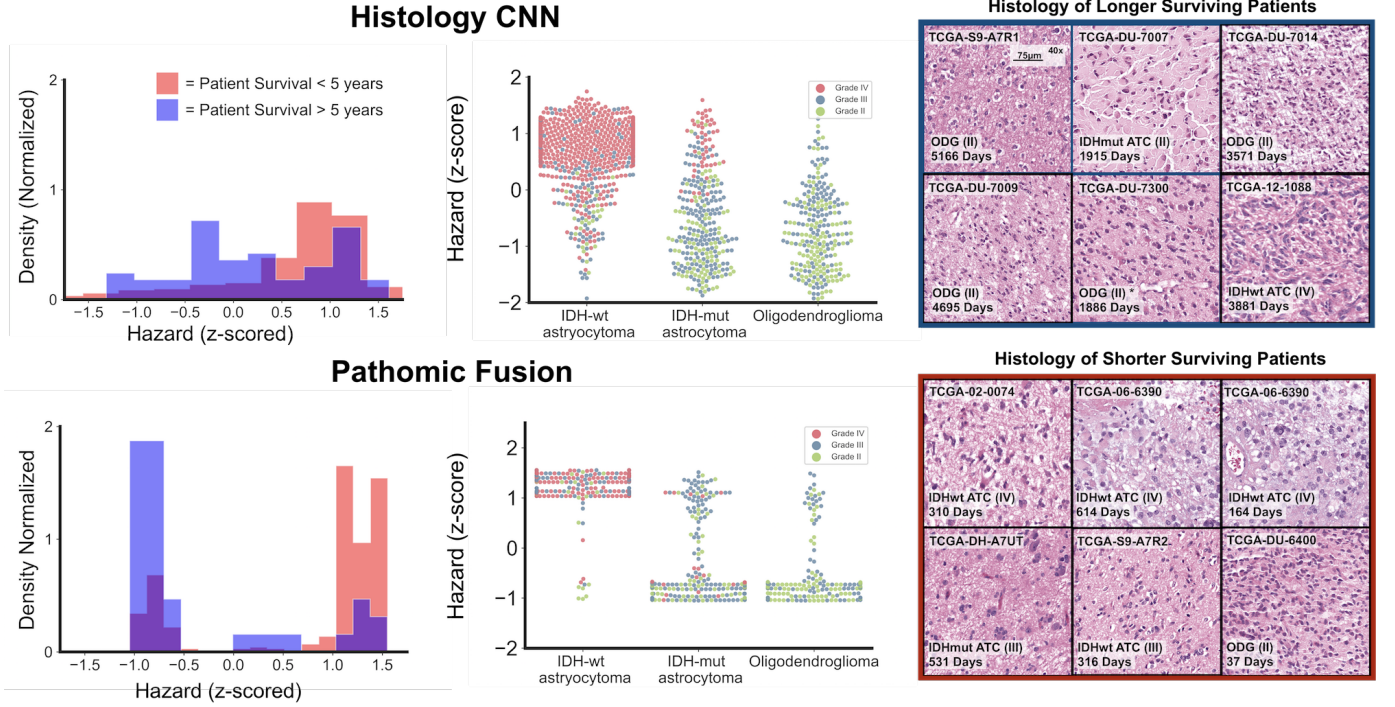


Fig. 3: Distribution of hazard predictions amongst shorter vs. longer surviving uncensored patients and molecular subtypes in Histology CNN and Pathomic Fusion. Patients are defined as shorter surviving if patient death is observed before 5 years of the first follow-up (shaded red), and longer surviving if patient death is observed after 5 years of the first follow-up (shaded blue). Pathomic Fusion predicts hazard in more concentrated clusters than Histology CNN, while the distribution of hazard predictions from Histology CNN have longer tails and are more varied across molecular subtypes. In analyzing the types of glioma in the three high density regions revealed from Pathomic Fusion, we see that these regions corroborate with the WHO paradigm for stratifying patients into IDHwt ATC, IDHmut ATC, and ODG (Appendix C, Table IV).

orientation, edge eccentricity and gray-level occurrence matrix of homogeneity (GLCM), which are used to describe abnormal features such as atypia, nuclear pleomorphism, abundant cellularity, and hyperchromatism. These features were used to form our node feature matrix X , with 12 features calculated in total.

Unsupervised Cell Feature Extraction using Contrastive Predictive Coding: Besides manually computed statistics, we also used an unsupervised technique known as contrastive predictive coding (CPC) [48]–[50] to extract 1024-dimensional features from tissue regions of size 64×64 centered around each cell in a spatial graph. Given a high-dimensional data sequence $\{x_t\}$ (256×256 image crop from the histology ROI), CPC is designed to capture high-level representations shared among different portions (64×64 image patches) of the complete signal. The encoder network g_{enc} transforms each data observation x_i into a low-dimensional representation z_i and learns via a contrastive loss whose optimization leads to maximizing the mutual information between the available context c_t , computed from a known portion of the encoded sequence $\{z_i\}, i \leq t$ and future observations $z_{t+k}, k > 0$. By minimizing the CPC objective, we are able to learn rich feature representations shared among various tissue regions that are specific to the cells in the underlying tissue site. Examples include the morphology and distinct arrangement of different cell types, inter-cellular interactions, and the microvascular

patterns surrounding each cell. To create CPC features for each cell, we encode 64×64 image patches centered over the centroid of each cell. These features are concatenated with our handcrafted features during cell graph construction.

Graph Convolutional Network: Similar to CNNs, GCNs learn abstracts feature representations for each feature in a node via message passing, in which nodes iteratively aggregate feature vectors from their neighborhood to compute a new feature vector at the next hidden layer in the network [31]. The representation of an entire graph can be obtained through pooling over all the nodes, which can then be used as input for tasks such as classification or survival outcome prediction. Such convolution and pooling operations can be defined as follows:

$$a_v^{(k)} = \text{AGGREGATE}^{(k)} \left(\left\{ h_u^{(k-1)} : u \in \mathcal{N}(v) \right\} \right)$$

$$h_v^{(k)} = \text{COMBINE}^{(k)} \left(h_v^{(k-1)}, a_v^{(k)} \right)$$

where $h_v^{(k)}$ is the feature vector of node v at the $k - 1$ -th iteration of the neighborhood aggregation, $a_v^{(k)}$ is the feature vector of node v at the next iteration, and AGGREGATE and COMBINE are functions for combining feature vectors between hidden layers. As defined in Hamilton *et al.*, we adopt the AGGREGATE and COMBINE definitions from GraphSAGE [28], which for a given node, represents the next node hidden layer as the concatenation of the current hidden layer with the neighborhood features:

$$a_v^{(k)} = \mathbf{MAX} \left(\left\{ \mathbf{ReLU} \left(W \cdot h_u^{(k-1)} \right), \forall u \in \mathcal{N}(v) \right\} \right)$$

$$h_v^{(k)} = W \cdot \left[h_v^{(k-1)}, a_v^{(k)} \right]$$

To learn accurate representations of the spatial distribution of nuclei, we adopt the self-attention pooling strategy (SAGPOOL) presented in Lee *et al.* [29], which allows the network to selectively focus on more important node features to better reflect the topology and community structure of the nuclei. The attention score $Z \in \mathcal{R}^{N \times 1}$ for nodes in G can be calculated as such:

$$Z = \sigma \left(\mathbf{SAGEConv} \left(X, A + A^2 \right) \right)$$

where X are the node features, A is the adjacency matrix, and SAGEConv is the convolution operator from GraphSAGE. To also aggregate information from multiple scales in the nuclei graph topology, we also adopt the hierarchical pooling strategy in Lee *et al.* [29]. Since we are constructing cell graphs on the entire 1024×1024 image, no patch averaging of predicted hazards needs to be performed. At the last hidden layer of our Graph Convolutional SNN, we pool the node features into a $\mathbf{h}_g \in \mathcal{R}^{32 \times 1}$ feature vector, which we use as an input to Pathomic Fusion.

C. Predicting Patient Outcomes from Molecular Profiles using Self-Normalizing Networks

Advances in next-generation sequencing data have allowed for the profiling of transcript abundance (mRNAseq), copy number variation (CNV), mutation status, and other molecular characterizations at the gene level, and have been frequently used to study survival outcomes in cancer. For example, isocitrate dehydrogenase 1 (IDH1) is a gene that is important for cellular metabolism, epigenetic regulation and DNA repair, with its mutation associated with prolonged patient survival in cancers such as glioma.

Our approach to deal with the challenges of using genomic data is to learn a low-dimensional feature-rich representation using a Feedforward Self-Normalizing Network [51]. Regular Feedforward networks that use batch normalization to normalize neuron activations to zero mean and unit variance are prone to SGD and stochastic regularization techniques such as Dropout, which is frequently used in low-sample size data to prevent overfitting. Self-Normalizing Networks (SNN), introduced by Klambauer *et al.* [51], replaces ReLU activation with SeLU to drive outputs after every layer towards zero mean and unit variance as long as the inputs are normalized. Combined with a modified regularization technique (Alpha Dropout) that maintains this self-normalizing property, SNN allows us to learn robust feature representations from genomics data by building deeper, well-regularized Feedforward networks that are otherwise prone to instabilities as a result of vanishing or explosive gradients. Our network architecture consists of four fully-connected layers followed by Exponential Linear Unit (ELU) activation and Alpha Dropout to ensure the self-normalization property. The last fully-connected layer is used to learn a representation $\mathbf{h}_n \in \mathcal{R}^{32 \times 1}$, which is used as input into our Pathomic Fusion (Fig. 1).

D. Multimodal Tensor Fusion via Kronecker Product and Gating-Based Attention

For multimodal data in cancer pathology, there exists a data heterogeneity gap in combining histology and genomic input - histology images are spatial distributed as (R, G, B) pixels in a two-dimensional grid, whereas cell graphs are defined as a set of nodes V with different sized neighborhoods and edges V , and genomic data is often represented as a one-dimensional vector of covariates. Our motivation for multimodal learning is that the inter-modality interactions between histology and genomic features would be able to improve patient stratification into subtypes and treatment groups. For example, in the refinement of histogenesis of glioma, though morphological characteristics alone do not correlate well with patient outcomes, their semantic importance in drawing decision boundaries is changed when conditioned on genomic biomarkers such as IDH1 mutation status and chromosomal 1p19q arm codeletion [52].

In this work, we aim to explicitly capture these important interactions using the Kronecker Product, which computes a multimodal tensor that models all feature interactions across different modalities. Following the construction of the three unimodal feature representations in the previous subsections, we build a multimodal representation using the Kronecker product of the histology image, cell graph, and genomic features ($\mathbf{h}_i, \mathbf{h}_g, \mathbf{h}_n$). The joint multimodal tensor computed by the matrix outer product of these feature vectors would capture important unimodal, bimodal and trimodal interactions of all features of these three modalities, shown in Fig. 1 and in the equation below:

$$\mathbf{h}_{\text{fusion}} = \begin{bmatrix} \mathbf{h}_i \\ 1 \end{bmatrix} \otimes \begin{bmatrix} \mathbf{h}_g \\ 1 \end{bmatrix} \otimes \begin{bmatrix} \mathbf{h}_n \\ 1 \end{bmatrix}$$

where \otimes is the outer product, and $\mathbf{h}_{\text{fusion}}$ is a differential multimodal tensor that forms in a 3D Cartesian space. In this computation, every neuron in the last hidden layer in the CNN is multiplied by every other neuron in the last hidden layer of the SNN, and subsequently multiplied with every other neuron in the last hidden layer of the GCN. To preserve unimodal and bimodal feature interactions when computing the trimodal interactions, we append 1 to each unimodal feature representation. For feature vectors of size $[33 \times 1]$, $[33 \times 1]$ and $[33 \times 1]$, the calculated multimodal tensor would have dimension $[33 \times 33 \times 33]$, where the unimodal features ($\mathbf{h}_i, \mathbf{h}_g, \mathbf{h}_n$) and bimodal feature interactions ($\mathbf{h}_i \otimes \mathbf{h}_g, \mathbf{h}_g \otimes \mathbf{h}_n, \mathbf{h}_i \otimes \mathbf{h}_n$) are defined along the outer dimension of the 3D tensor, and the trimodal interactions (captured as $\mathbf{h}_i \otimes \mathbf{h}_g \otimes \mathbf{h}_n$) in the inner dimension of the 3D tensor (Fig. 1). Following the computation of this joint representation, we learn a final network using fully-connected layers using the multimodal tensor as input, supervised with the previously defined Cox objective for survival outcome prediction and cross-entropy loss for grade classification. Our multimodal network is initialized with pretrained weights from the unimodal networks, followed by end-to-end fine-tuning of the Histology GCN and Genomic SNN.

To decrease the impact of noisy unimodal features during multimodal training, we employed a gating-based attention mechanism that controls the expressiveness of features of

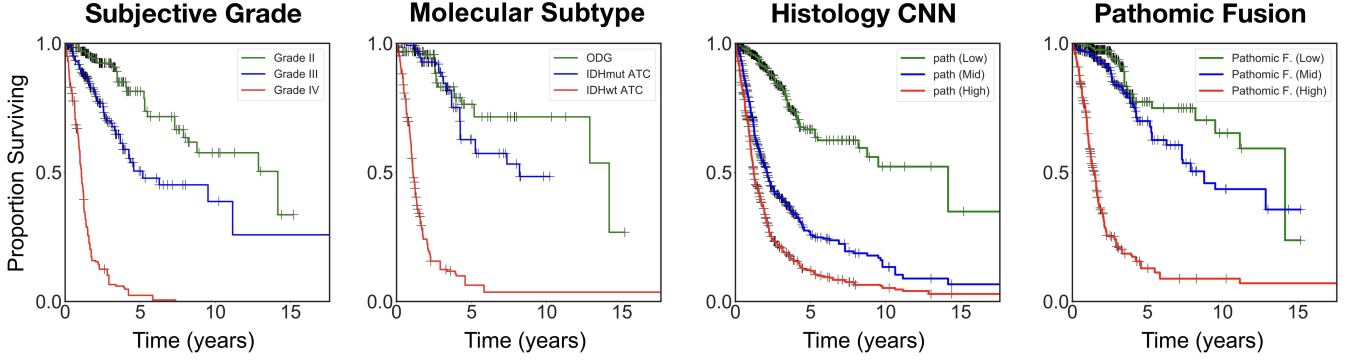


Fig. 4: Kaplan-Meier comparative analysis of using grade, molecular subtype, Histology CNN and Pathomic Fusion in stratifying patient outcomes. Hazard predictions from Pathomic Fusion show better stratification of mid-to-high risk patients than Histology CNN, and low-to-mid risk patients than molecular subtyping, which follows the WHO paradigm. Low/mid/high risk are defined by the 33-66 percentile of hazard predictions. Overlaid Kaplan-Meier estimates of our network predictions with WHO Grading is shown in the Appendix (Fig. 8).

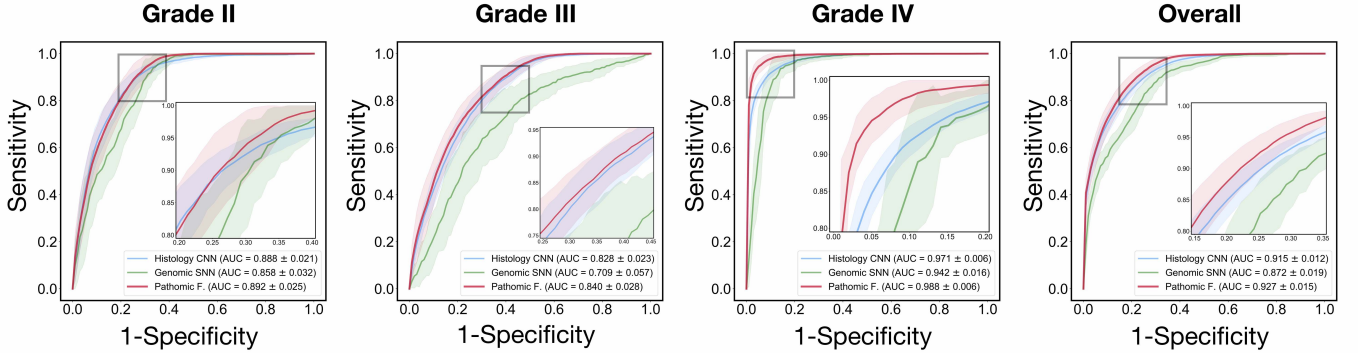


Fig. 5: Comparative analysis of AUC curves for histology, genomics and Pathomic Fusion in grade classification. The confidence interval is representative of the 15-fold cross validation. Since grade is usually determined via histology, our Genomic SNN that uses only CNV, gene mutation and chromosome deletion is not predictive of grade. Pathomic Fusion has greater AUCs in all cases, and performs particularly well on grade IV potentially because IDH mutation and 1p19q co-deletion from the genomic profile aid in discriminating Grade IV astrocytomas and Grade II/III oligodendrogliomas.

each modality. In fusing histology image, cell graph, and genomic features, some of the captured features may have high collinearity, in which employing a gating mechanism can reduce the size of the feature space before computing the Kronecker Product. For a modality m with a unimodal feature representation \mathbf{h}_m , we learn a linear transformation $W_{ign \rightarrow m}$ of modalities $\mathbf{h}_i, \mathbf{h}_g, \mathbf{h}_n$ that would score the relative importance of each feature in m , denoted as \mathbf{z}_m in the equation below.

$$\mathbf{h}_{m,\text{gated}} = \mathbf{z}_m * \mathbf{h}_m, \forall m \in \{i, g, n\}$$

$$\text{where, } \mathbf{h}_m = \text{ReLU}(W_m \cdot \mathbf{h}_m)$$

$$\mathbf{z}_m = \sigma(W_{ign \rightarrow m} \cdot [\mathbf{h}_i, \mathbf{h}_g, \mathbf{h}_n])$$

\mathbf{z}_m can be interpreted as an attention weight vector, in which modalities i, g, n attend over each feature in modality m . W_m and $W_{ign \rightarrow m}$ are weight matrix parameters we learn for feature gating. After taking the softmax probability, we take the element-wise product of features \mathbf{h}_m and scores \mathbf{z}_m to calculate the gated representation.

IV. EXPERIMENTAL SETUP

A. Data Description

The data obtained from the TCGA-GBM and TCGA-LGG project contains curated paired samples of diagnostic whole slide images and genomic information with ground-truth survival outcome and histologic grade labels. The histology region-of-interests from the diagnostic slides were curated from [23] and are of size 1024×1024 , and were normalized using sparse stain normalization [53] to match all images to a standard H&E histology image. Multiple region-of-interests (ROIs) from diagnostic slides were obtained for some patients, creating a total of 1505 images for 769 patients. 360 genomic features from gene CNV (79), mutation status (1), mRNAseq expression (240) were curated from the TCGA and the cBioPortal [54] for each patient. Additional details regarding data alignment of histology and genomic data for training are found in the implementation details (Appendix B).

B. Quantitative Study

The current World Health Organization (WHO) Paradigm for glioma classification stratifies diffuse gliomas based on

TABLE I: Comparative analysis of Pathomic Fusion on survival prediction and grade classification in a 15-fold cross validation.

Model	c-Index	P Value	AUC \uparrow	AP \uparrow	F1-Score (Micro) \uparrow	F1-Score (Grade IV)
Cox (Grade)	0.738 ± 0.013	$9.65\text{e-}7$	-	-	-	-
Cox (Subtype)	0.760 ± 0.011	$2.92\text{e-}4$	-	-	-	-
Cox (Grade+Subtype)	0.777 ± 0.013	$4.75\text{e-}09$	-	-	-	-
Histology CNN	0.750 ± 0.010	$4.92\text{e-}17$	0.915 ± 0.007	0.852 ± 0.012	0.747 ± 0.013	0.901 ± 0.006
Histology GCN	0.722 ± 0.014	$2.68\text{e-}12$	0.872 ± 0.009	0.793 ± 0.014	0.672 ± 0.017	0.861 ± 0.010
Genomic SNN	0.808 ± 0.014	$8.92\text{e-}18$	0.872 ± 0.011	0.761 ± 0.018	0.670 ± 0.014	0.882 ± 0.015
SCNN (Histology Only) [23])	0.754	$2.08\text{e-}61$	-	-	-	-
GSCNN (Histology + IDH1/1p19q) [23])	0.781	$3.08\text{e-}64$	-	-	-	-
Pathomic Fusion (GCN \otimes SNN)	0.812 ± 0.010	$1.53\text{e-}10$	0.913 ± 0.008	0.838 ± 0.014	0.742 ± 0.017	0.923 ± 0.010
Pathomic Fusion (CNN \otimes SNN)	0.820 ± 0.009	$2.34\text{e-}12$	0.925 ± 0.008	0.865 ± 0.014	0.754 ± 0.015	0.921 ± 0.008
Pathomic Fusion (CNN \otimes GCN \otimes SNN)	0.826 ± 0.009	$6.95\text{e-}13$	0.927 ± 0.009	0.866 ± 0.015	0.762 ± 0.018	0.932 ± 0.009

morphological and molecular characteristics: glial cell type (astrocytoma, oligodendroglioma), IDH1 gene mutation status and 1p19q chromosome codeletion status [52]. WHO Grading is made by the manual interpretation of histology using pathological determinants for malignancy (WHO Grades II, III, and IV). These characteristics form three categories of gliomas which have been extensively correlated with survival: 1) IDH-wildtype astrocytomas (IDHwt ATC), 2) IDH-mutant astrocytomas (IDHmut ATC), and 3) IDH-mutant and 1p/19q-codeleted oligodendrogliomas (ODG). IDHwt ATCs (predominantly WHO grades III and IV) have been shown to have the worst patient survival outcomes, while IDHmut ATCs (mixture of WHO Grades II, III, and IV) and ODGs (predominantly WHO Grades II and III) have more favorable outcomes (listed in increasing order) [52]. As a baseline against standard statistical approaches / WHO paradigm for survival outcome prediction, we trained Cox Proportion Hazard Models using molecular subtypes and histologic grade labels as covariates.

In our experimentation, we conducted a rigorous ablation study comparing model configurations and fusion strategies in a 15-fold cross validation on two supervised learning tasks: survival outcome prediction (Appendix A) and cancer grade classification. For each task, we trained six different model configurations from the combination of available modalities in the dataset. First, we trained three different unimodal networks: 1) a CNN for in histology image input (Histology CNN), 2) a GCN for cell graph input (Histology GCN), and 3) a SNN for genomic features input (Genomic SNN). For survival outcome prediction, our Genomic SNN used not only IDH mutation and 1p19q codeletion status as covariates, but also mRNAseq, CNV, and mutations for frequently mutated genes. For cancer grade classification, we did not use mRNAseq expression due to missing data, lack of paired training examples, and because grade is solely determined from histopathologic appearance. After training the unimodal networks, we trained three different configurations of Pathomic Fusion: 1) GCN \otimes SNN, 2) CNN \otimes SNN, 3) GCN \otimes CNN \otimes SNN. We compare our fusion approach to internal benchmarks and the previous state-of-the-art [23], which integrates IDH mutation and 1p19q codeletion status into a VGG19 CNN at the last hidden layers of the networks. To test for ensembling, we train multimodal networks that fused histology data with histology data, and genomic features with genomic features. In total, we trained 270 models in a 15-fold cross validation with train-test splits obtained from

the supplement of [23]. Implementation and training details for all networks are described in detail in Appendix A and B.

We evaluate our method both quantitatively with standard metrics of the two learning tasks, and qualitatively in how well these networks can subtype gliomas and stratify patient outcomes. For survival analysis, we evaluate all models using the Concordance Index (c-Index), which is defined as the fraction of all pairs of samples whose predicted survival times are correctly ordered among all uncensored samples (Table I). Additionally, we show Kaplan–Meier estimates of overall survival among patients from subjective histologic grading and subtyping, molecular subtyping, objective subtyping via Histology CNN, and objective subtyping via Pathomic Fusion (Fig. 4). To further understand the improvement made by Pathomic Fusion over Histology CNN, we analyze the distribution of hazard predictions for uncensored patients across molecular subtypes and low vs. high risk cohorts (Fig. 3). For grade classification, we evaluate our networks using Area Under the Curve (AUC), Average Precision (AP), F1-Score (micro-averaged across all classes), F1-Score (WHO Grade IV class only), and show ROC curves (Fig. 4).

V. RESULTS AND DISCUSSION

A. Pathomic Fusion Outperforms Unimodal Networks and the WHO Paradigm

In combining histology image, cell graph, and genomic features via Pathomic Fusion, our approach outperforms Cox models, unimodal networks, and previous deep learning-based feature fusion approaches on both survival outcome prediction and cancer grade classification (Table I). On survival outcome prediction, Pathomic Fusion outperforms the WHO paradigm and the previous state-of-the-art (concatenation-based fusion [23]) with **6.31%** and **5.76%** improvements respectively, reaching a c-Index of **0.826** (P Value = $6.95\text{e-}13$) and AUC of **0.927**. In addition, we demonstrate that multimodal networks are able to consistently improve upon their unimodal baselines, with the Genomic SNN benefiting from the addition of histology image and cell graph modalities as input with 2.28% improvement. We also demonstrate that these improvements are not due to network ensembling, as inputting same modality twice into Pathomic Fusion caused overfitting and decreased performance (Appendix C, Table II). On grade classification, we see similar improvement with Pathomic Fusion with increases of 1.31% AUC, 1.64% average precision, 2.01% F1-score

(micro), and 3.44% (Grade IV) over Histology CNN, which is consistent with performance increases found in multimodal learning literature for conventional vision tasks [18].

B. Parameter-Efficient Feature Fusion using Cell Graphs and Genomic Features

From our results, morphometric feature extraction from histology-based cell graphs using GCNs is a parameter-efficient approach towards solving tasks such as survival outcome prediction. Though CNN- and GCN-based histology feature extraction would learn similar morphological features, our CNN (VGG19) uses $13\times$ the parameters are our GCN. Evaluating Histology CNN also required the ensembling of patch predictions from a 1024×1024 ROI, whereas Histology GCNs were able to train with the entire ROI as cell graphs. In our results, we show that while Histology CNN performs better than Histology GCN, the improvements in fusing with genomic features are in the same ranges for c-Index, AUC, and F1-Score (Grade IV) performance increases (Appendix C, Table III). On grade classification, the integration of GCNs in Pathomic Fusion (GCN \otimes CNN) was able to substantially improve Histology GCN / Genomic SNN alone with a 4.70% performance increase on AUC and 7.07% performance increase on F1-Score (Grade IV). Our results suggest that cell graphs are a powerful alternative to histology images for extracting morphological features, and the 13-fold decrease in the number of trainable parameters allows GCNs to learn from larger spatial resolutions of histology images.

C. Objective and Integrative Histology-Based Prognosis using Pathomic Fusion

To investigate the ability of Pathomic Fusion for improving objective histology-based patient stratification, we plot Kaplan-Meier (KM) curves of our trained networks against the WHO paradigm which uses molecular subtyping (Fig. 4). Similar to [23], we observe that the segregation of risk categories captured by Pathomic Fusion are similar to that of the three defined glioma subtypes (IDHwt ATC, IDHmut ATC, ODG) that correlate with survival. In comparing Pathomic Fusion to Histology CNN, Pathomic Fusion was able to discriminate intermediate and high risk patients better than Histology CNN but was unable to clearly define low and intermediate risk patients, which corroborates with known literature that WHO Grades II and III are more difficult to distinguish than Grades III and IV [52]. Similar confusion in discriminating low and intermediate risk patients is also shown in the KM estimates of molecular subtypes.

Additional comparisons between Histology CNN and Pathomic Fusion are made in analyzing distribution of predicted hazard scores for patients in low vs. high surviving cohorts (Fig. 3). Qualitatively, we observe that Pathomic Fusion is able to predict more concentrated cluster assignments of hazard than Histology CNN, as seen in the 3 high density regions: $[-1.0, -0.5]$, $[1.0, 1.25]$ and $[1.25, 1.5]$, and that the distribution of predictions made by Histology CNN are more skewed and spread out in each cohort. In analyzing the high density regions elucidated by Pathomic Fusion, we see that these regions

strongly corroborate with the WHO Paradigm for stratifying gliomas into IDHwt ATC, IDHmut ATC, and ODG.

VI. CONCLUSION

Though quantitative information from genomic data allows for more objective-based analyses, the current WHO paradigm for prognosis of cancers such as glioma still depends on the subjective interpretation of histology images, which is known to suffer from high intra- and interobserver variability. In this work, we present Pathomic Fusion, a novel framework for integrating histology image, cell graph, and genomic features for objective-based cancer diagnosis and prognosis. We extract morphological features from histology images using two different views: image-based features from CNNs and morphometric graph-based features from GCNs, and fuse these features using the Kronecker Product and a gating-based attention mechanism. We validate our approach on the TCGA-GBM and TCGA-LGG projects, and demonstrate an improvement over the current state-of-the-art in survival outcome prediction using histology images. Future work would include curating more paired histology and genomic data, and conducting a pan-cancer study on the Dana Farber OncoPanel Platform.

ACKNOWLEDGEMENTS

The authors would like to thank generous computing support from the Nvidia GPU grant program and Google Cloud. R.J.C. is funded by the National Science Foundation Graduate Fellowship and the NIH NHGRI T32 training program.

REFERENCES

- [1] P. Y. Wen and S. Kesari, "Malignant gliomas in adults," *New England Journal of Medicine*, vol. 359, no. 5, pp. 492–507, Jul. 2008.
- [2] L. Nayak, E. Q. Lee, and P. Y. Wen, "Epidemiology of brain metastases," *Current Oncology Reports*, vol. 14, no. 1, pp. 48–54, Oct. 2011.
- [3] K. Aldape, G. Zadeh, S. Mansouri, G. Reifenberger, and A. von Deimling, "Glioblastoma: pathology, molecular mechanisms and markers," *Acta Neuropathologica*, vol. 129, no. 6, pp. 829–848, May 2015.
- [4] A. Olar and K. D. Aldape, "Using the molecular classification of glioblastoma to inform personalized treatment," *The Journal of Pathology*, vol. 232, no. 2, pp. 165–177, Dec. 2013.
- [5] J. Shanes, J. Ghali, M. Billingham, V. Ferrans, J. Fenoglio, W. Edwards, C. Tsai, J. Saffitz, J. Isner, and S. Furner, "Interobserver variability in the pathologic interpretation of endomyocardial biopsy results," *Circulation*, vol. 75, no. 2, pp. 401–405, 1987.
- [6] P. Courtiol, C. Maussion, M. Moarii, E. Pronier, S. Pilcer, M. Sefta, and et al., "Deep learning-based classification of mesothelioma improves prediction of patient outcome," *Nature medicine*, vol. 25, no. 10, pp. 1519–1525, 2019.
- [7] O. Gallego, "Nonsurgical treatment of recurrent glioblastoma," *Current Oncology*, vol. 22, no. 4, p. 273, May 2015.
- [8] B. Yener, "Cell-graphs: image-driven modeling of structure-function relationship," *Communications of the ACM*, vol. 60, no. 1, pp. 74–84, 2016.
- [9] S. Gadiya, D. Anand, and A. Sethi, "Histographs: Graphs in histopathology," *arXiv preprint arXiv:1908.05020*, 2019.
- [10] J. Wang, R. J. Chen, M. Y. Lu, A. Baras, and F. Mahmood, "Weakly supervised prostate tma classification via graph convolutional networks," *arXiv preprint arXiv:1910.13328*, 2019.
- [11] S. Zuo, X. Zhang, and L. Wang, "A RNA sequencing-based six-gene signature for survival prediction in patients with glioblastoma," *Scientific Reports*, vol. 9, no. 1, Feb. 2019.
- [12] TCGA et al., "Integrated genomic analyses of ovarian carcinoma," *Nature*, vol. 474, no. 7353, p. 609, 2011.
- [13] S. Yousefi, F. Amrollahi, M. Amgad, C. Dong, J. E. Lewis, C. Song, and et al., "Predicting clinical outcomes from large scale cancer genomic profiles with deep survival models," *Scientific Reports*, vol. 7, no. 1, Sep. 2017.

- [14] Z. Huang, X. Zhan, S. Xiang, T. S. Johnson, B. Helm, C. Y. Yu, and et al., "Salmon: Survival analysis learning with multi-omics neural networks on breast cancer," *Frontiers in genetics*, vol. 10, p. 166, 2019.
- [15] J. Ngiam, A. Khosla, M. Kim, J. Nam, H. Lee, and A. Y. Ng, "Multimodal deep learning," in *Proceedings of the 28th international conference on machine learning (ICML-11)*, 2011, pp. 689–696.
- [16] H. Suresh, N. Hunt, A. Johnson, L. A. Celi, P. Szolovits, and M. Ghassemi, "Clinical intervention prediction and understanding with deep neural networks," in *Machine Learning for Healthcare Conference*, 2017, pp. 322–337.
- [17] J.-H. Kim, K.-W. On, W. Lim, J. Kim, J.-W. Ha, and B.-T. Zhang, "Hadamard product for low-rank bilinear pooling," *arXiv preprint arXiv:1610.04325*, 2016.
- [18] A. Zadeh, M. Chen, S. Poria, E. Cambria, and L.-P. Morency, "Tensor fusion network for multimodal sentiment analysis," in *Proceedings of the 2017 Conference on Empirical Methods in Natural Language Processing*. Association for Computational Linguistics, 2017.
- [19] V. Subramanian, B. Chidester, J. Ma, and M. N. Do, "Correlating cellular features with gene expression using cca," in *2018 IEEE 15th International Symposium on Biomedical Imaging (ISBI 2018)*. IEEE, 2018, pp. 805–808.
- [20] I. Carmichael and J. Marron, "Joint and individual analysis of breast cancer histologic images and genomic covariates," *arXiv preprint arXiv:1912.00434*, 2019.
- [21] N. Coudray, P. S. Ocampo, T. Sakellaropoulos, N. Narula, M. Snuderl, Fenyő, and et al., "Classification and mutation prediction from non-small cell lung cancer histopathology images using deep learning," *Nature medicine*, vol. 24, no. 10, p. 1559, 2018.
- [22] J. N. Kather, A. T. Pearson, N. Halama, D. Jäger, J. Krause, S. H. Loosen, and et al., "Deep learning can predict microsatellite instability directly from histology in gastrointestinal cancer," *Nature medicine*, p. 1, 2019.
- [23] P. Mobadersany, S. Yousefi, M. Amgad, D. A. Gutman, J. S. Barnholtz-Sloan, J. E. V. Vega, and et al., "Predicting cancer outcomes from histology and genomics using convolutional networks," *Proceedings of the National Academy of Sciences*, vol. 115, no. 13, pp. E2970–E2979, Mar. 2018.
- [24] T. Baltrusaitis, C. Ahuja, and L.-P. Morency, "Multimodal machine learning: A survey and taxonomy," *IEEE Transactions on Pattern Analysis and Machine Intelligence*, vol. 41, no. 2, pp. 423–443, Feb. 2019.
- [25] A. Cheerla and O. Gevaert, "Deep learning with multimodal representation for pancancer prognosis prediction," *Bioinformatics*, vol. 35, no. 14, pp. i446–i454, Jul. 2019.
- [26] W. Shao, Z. Han, J. Cheng, L. Cheng, T. Wang, L. Sun, Z. Lu, J. Zhang, D. Zhang, and K. Huang, "Integrative analysis of pathological images and multi-dimensional genomic data for early-stage cancer prognosis," *IEEE Transactions on Medical Imaging*, 2019.
- [27] S. Doyle, M. Hwang, K. Shah, A. Madabhushi, M. Feldman, and J. Tomaszewski, "Automated grading of prostate cancer using architectural and textural image features," in *2007 4th IEEE International Symposium on Biomedical Imaging: From Nano to Macro*. IEEE, 2007, pp. 1284–1287.
- [28] W. Hamilton, Z. Ying, and J. Leskovec, "Inductive representation learning on large graphs," in *Advances in Neural Information Processing Systems*, 2017, pp. 1024–1034.
- [29] J. Lee, I. Lee, and J. Kang, "Self-attention graph pooling," *arXiv preprint arXiv:1904.08082*, 2019.
- [30] M. Defferrard, X. Bresson, and P. Vandergheynst, "Convolutional neural networks on graphs with fast localized spectral filtering," in *Advances in neural information processing systems*, 2016, pp. 3844–3852.
- [31] T. N. Kipf and M. Welling, "Semi-supervised classification with graph convolutional networks," *arXiv preprint arXiv:1609.02907*, 2016.
- [32] Y. Zhou, S. Graham, N. A. Koohbanani, M. Shaban, P.-A. Heng, and N. Rajpoot, "Cgc-net: Cell graph convolutional network for grading of colorectal cancer histology images," *arXiv preprint arXiv:1909.01068*, 2019.
- [33] A. Marusyk, V. Almendro, and K. Polyak, "Intra-tumour heterogeneity: a looking glass for cancer?" *Nature Reviews Cancer*, vol. 12, no. 5, pp. 323–334, Apr. 2012.
- [34] H. Yang, J.-Y. Kim, H. Kim, and S. P. Adhikari, "Guided soft attention network for classification of breast cancer histopathology images," *IEEE transactions on medical imaging*, 2019.
- [35] C. T. Sari and C. Gunduz-Demir, "Unsupervised feature extraction via deep learning for histopathological classification of colon tissue images," *IEEE transactions on medical imaging*, vol. 38, no. 5, pp. 1139–1149, 2018.
- [36] P. Bandi, O. Geessink, Q. Manson, M. Van Dijk, M. Balkenhol, M. Hermesen, and et al., "From detection of individual metastases to classification of lymph node status at the patient level: the camelyon17 challenge," *IEEE transactions on medical imaging*, vol. 38, no. 2, pp. 550–560, 2018.
- [37] E. Guadagno, G. Borrelli, M. Califano, G. Calì, D. Solari, and M. D. B. D. Caro, "Immunohistochemical expression of stem cell markers CD44 and nestin in glioblastomas: Evaluation of their prognostic significance," *Pathology - Research and Practice*, vol. 212, no. 9, pp. 825–832, Sep. 2016.
- [38] V. E. Mikkelsen, A. L. Stensjøen, E. M. Berntsen, I. S. Nordrum, Ø. Salvesen, O. Solheim, and S. H. Torp, "Histopathologic features in relation to pretreatment tumor growth in patients with glioblastoma," *World Neurosurgery*, vol. 109, pp. e50–e58, Jan. 2018.
- [39] P. Naylor, M. Laé, F. Reyat, and T. Walter, "Segmentation of nuclei in histopathology images by deep regression of the distance map," *IEEE transactions on medical imaging*, vol. 38, no. 2, pp. 448–459, 2018.
- [40] J. Xu, L. Xiang, Q. Liu, H. Gilmore, J. Wu, J. Tang, and A. Madabhushi, "Stacked sparse autoencoder (ssae) for nuclei detection on breast cancer histopathology images," *IEEE transactions on medical imaging*, vol. 35, no. 1, pp. 119–130, 2015.
- [41] H. Su, F. Xing, and L. Yang, "Robust cell detection of histopathological brain tumor images using sparse reconstruction and adaptive dictionary selection," *IEEE transactions on medical imaging*, vol. 35, no. 6, pp. 1575–1586, 2016.
- [42] Z. Jia, X. Huang, I. Eric, C. Chang, and Y. Xu, "Constrained deep weak supervision for histopathology image segmentation," *IEEE transactions on medical imaging*, vol. 36, no. 11, pp. 2376–2388, 2017.
- [43] N. Kumar, R. Verma, S. Sharma, S. Bhargava, A. Vahadane, and A. Sethi, "A dataset and a technique for generalized nuclear segmentation for computational pathology," *IEEE Transactions on Medical Imaging*, vol. 36, no. 7, pp. 1550–1560, Jul. 2017.
- [44] F. Mahmood, D. Borders, R. Chen, G. McKay, K. J. Salimian, A. Baras, , and N. J. Durr, "Adversarial training for multi-organ nuclei segmentation in computational pathology images," in *IEEE Transactions on Medical Imaging*, 2018.
- [45] I. Goodfellow, J. Pouget-Abadie, M. Mirza, B. Xu, D. Warde-Farley, S. Ozair, A. Courville, and Y. Bengio, "Generative adversarial nets," in *Advances in neural information processing systems*, 2014, pp. 2672–2680.
- [46] P. Isola, J.-Y. Zhu, T. Zhou, and A. A. Efros, "Image-to-image translation with conditional adversarial networks," in *Proceedings of the IEEE conference on computer vision and pattern recognition*, 2017, pp. 1125–1134.
- [47] M. Muja and D. G. Lowe, "Fast approximate nearest neighbors with automatic algorithm configuration." *VISAPP (1)*, vol. 2, no. 331–340, p. 2, 2009.
- [48] A. v. d. Oord, Y. Li, and O. Vinyals, "Representation learning with contrastive predictive coding," *arXiv preprint arXiv:1807.03748*, 2018.
- [49] O. J. Hénaff, A. Razavi, C. Doersch, S. Eslami, and A. v. d. Oord, "Data-efficient image recognition with contrastive predictive coding," *arXiv preprint arXiv:1905.09272*, 2019.
- [50] M. Y. Lu, R. J. Chen, J. Wang, D. Dillon, and F. Mahmood, "Semi-supervised histology classification using deep multiple instance learning and contrastive predictive coding," *arXiv preprint arXiv:1910.10825*, 2019.
- [51] G. Klambauer, T. Unterthiner, A. Mayr, and S. Hochreiter, "Self-normalizing neural networks," in *Advances in neural information processing systems*, 2017, pp. 971–980.
- [52] D. N. Louis, A. Perry, G. Reifenberger, A. von Deimling, D. Figarella-Branger, W. K. Cavenee, and et al., "The 2016 world health organization classification of tumors of the central nervous system: a summary," *Acta Neuropathologica*, vol. 131, no. 6, pp. 803–820, May 2016.
- [53] A. Vahadane, T. Peng, A. Sethi, S. Albarqouni, L. Wang, M. Baust, and et al., "Structure-preserving color normalization and sparse stain separation for histological images," *IEEE Transactions on Medical Imaging*, vol. 35, no. 8, pp. 1962–1971, Aug. 2016.
- [54] E. Cerami, , J. Gao, U. Dogrusoz, B. E. Gross, S. O. Sumer, B. A. Aksoy, and et al., "The cBio cancer genomics portal: An open platform for exploring multidimensional cancer genomics data: Figure 1." *Cancer Discovery*, vol. 2, no. 5, pp. 401–404, May 2012.
- [55] D. R. Cox, "Regression models and life-tables," *Journal of the Royal Statistical Society: Series B (Methodological)*, vol. 34, no. 2, pp. 187–202, 1972.
- [56] W. H. Wong, "Theory of partial likelihood," *The Annals of Statistics*, vol. 14, no. 1, pp. 88–123, Mar. 1986.
- [57] D. P. Kingma and J. Ba, "Adam: A method for stochastic optimization," *arXiv preprint arXiv:1412.6980*, 2014.

APPENDIX A. DEEP LEARNING-BASED SURVIVAL ANALYSIS

Survival analysis is a task that models the time to an event, where the outcome of the event is not always observed [55]. Such events are called censored, in which the date of the last known encounter is used as a lower bound of the survival time. For the task of cancer survival outcome prediction, an uncensored event would be patient death, and a censored event would include either patient survival or last known follow-up.

Let T be a continuous random variable that represents patient survival time, and the survival function $S(t) = P(T \geq t_0)$ be the probability of a patient surviving longer than time t_0 . We can denote the probability that an event occurs instantaneously at a time t (after t_0) as the hazard function $\lambda(t)$. Integrating the hazard function over the time between t and t_0 gives us the survival function [55].

$$\lambda(t) = \lim_{\partial t \rightarrow 0} \frac{P(t \leq T \leq t + \partial t | T \geq t)}{\partial t}, S(t) = \exp \left(- \int_0^t \lambda(x) \partial x \right).$$

The most common semi-parametric approach for estimating the hazard function is the Cox proportion hazards model, which assumes that the hazard function can be parameterized as an exponential linear function $\lambda(t|x) = \lambda_0(t)e^{\beta x}$, where $\lambda_0(t)$ is the baseline hazard that describes how the risk of an event changes over time, β are model parameters that describe how the hazard varies with covariates / features X of a patient. In the original model, the baseline hazard $\lambda_0(t)$ is left unspecified, making it difficult to estimate β , however, the Cox partial log-likelihood can be derived that expresses the likelihood of an event to be observed at time t for β, X [56].

$$l(\beta, X) = - \sum_{i \in U} \left(X_i \beta - \log \sum_{j \in R_i} e^{X_j \beta} \right), \frac{\partial l(\beta, X)}{\partial X_i} = \delta(i) \beta - \sum_{j \in R_i} \frac{\beta e^{X_j \beta}}{\sum_{k \in R_i} e^{X_k \beta}}$$

where U is the set of uncensored patients, R_i is the set of patients whose time of death or last follow-up is later than i . From the partial log-likelihood, β can be estimated using iterative optimization algorithms such as Newton-Raphson or Stochastic Gradient Descent. To train deep networks for survival analysis, features from the hidden layer are used as covariates in the Cox model, with the derivative of the partial log-likelihood used as error during back-propagation.

APPENDIX B. IMPLEMENTATION DETAILS

Data Missingness and Alignment

Aligning histology region-of-interests with genomic information in the TCGA-LGG and TCGA-GBM projects (419 and 350 patients respectively) required careful handling of missing and duplicate values for the different tasks of survival outcome prediction. For each patient, 1-3 1024×1024 histology ROIs from diagnostic slides, and CNV data from 79 genes were curated from the TCGA. Genes curated include EGFR, MDM4, MGMT, MYC and BRAF, which are implicated in oncogenic processes such as angiogenesis, apoptosis, cell growth, and differentiation. Of the 769 patients, 72 patients have missing molecular subtype (IDH mutation and 1p19q codeletion), 33 patients have missing histological subtype and grade labels, and 256 patients have missing mRNAseq data for the top 240 differentially expressed genes from cBioPortal (Fig. 6) [54]. Depending on the task (survival prediction vs. grade classification) and combination of modalities used (histology vs. genomic vs. histology+genomic), different subsets of the data were used to train the unimodal and multimodal networks. Because multiple ROIs from diagnostic slides were obtained for some patients, each image was treated as a single data point in cross-validation, with the genomic and ground-truth label information copied over. A 15-fold Monte-carlo cross-validation was conducted using the same train-test splits as the supplement of [23], which were generated randomly with 80% training and 20% testing (split by TCGA ID).

Network Architectures

Three different network architectures were used to process the three modalities in our problem: 1) a VGG19 CNN with batch normalization for histology images, 2) a GCN for cell spatial graphs, and 3) a Feedforward Self-Normalizing Network for molecular profiles. The VGG19 network consists of 16 convolutional, 3 fully connected and 5 max pooling layers, with 512×512 sized images used as input. Dropout probabilities of 0.25 were applied after the first two fully connected layers (of size

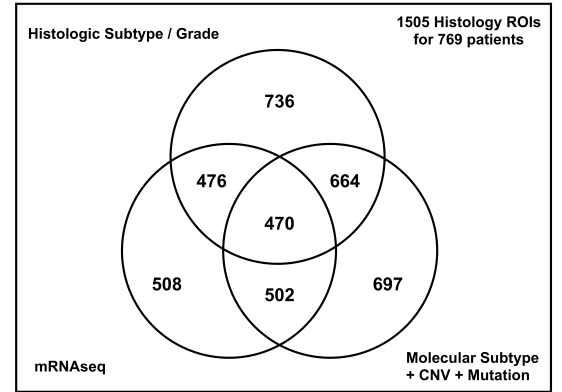


Fig. 6: Diagram describing missing data in the TCGA-glioma project. Because not all genomic features are available for all patients, Pathomic Fusion was trained with different subsets of the data than the unimodal networks for both survival outcome prediction and grade classification.

1024), with a mild dropout ($p=0.05$) applied after the last hidden layer (of size 32). Our GCN consisted of 3 GraphSAGE and Self-Attention Pooling layers with hidden dimension 128, followed by two linear layers of size 128 and 32. Lastly, our Genomic SNN consists of 4 consecutive blocks of fully-connected layers with dimensions [64, 48, 32, 32], ELU activation, and Alpha Dropout. For survival outcome prediction, all networks were activated using the Sigmoid function, with the output scaled to be between -3 and 3. For grade classification, all networks were activated using the Log Softmax to compute scores for each of the 3 WHO Grades.

Our multimodal network architectures consist of two components: 1) Gating-based Modality Attention, and 2) fusion by Kronecker Product. Each modality was gated using three linear layers, with the second linear layer used to compute the attention scores. For survival outcome prediction, the genomic modality was used to gate over the image and graph modalities, while for grade classification, the histology image modality was used to gate over the genomic and graph modality. Additional dimension reduction of the gated unimodal feature representations was performed to reduce the output size of the Kronecker product feature space in the trimodal network. In our trimodal network, for survival outcome prediction, the first and third linear layers for the genomic modality have 32 hidden units to maintain the feature map dimension, with the linear layers in the image and graph modalities having 16 hidden units in order to transform the feature representations into a lower dimension. For grade classification, we maintained the feature dimension of our histology image modality instead, and reduced the dimension of the graph and genomic modalities. No feature dimension reduction was done in bimodal networks in any tasks. For feature fusion, the Kronecker product of the respective unimodal feature representations for each modality was computed, creating feature maps of size: $[33 \times 33]$, $[33 \times 33]$, $[33 \times 17 \times 17]$ for our $\text{CNN} \otimes \text{SNN}$, $\text{GCN} \otimes \text{SNN}$, and $\text{CNN} \otimes \text{GCN} \otimes \text{SNN}$. To use the unperturbed unimodal features, we appended 1 to each feature vector before computing the Kronecker Product. Dropout layers with probability ($p = 0.25$) were inserted after gating and computing the multimodal tensor.

Training Details

The training code was implemented in PyTorch 1.3.0 and PyTorch Geometric 1.3.0. Resources used in our experimentation include 12 Nvidia GeForce RTX 2080 Tis on local workstations, and 2 Nvidia Tesla V100s on Google Cloud. The Histology CNN was initialized using pretrained weights from ImageNet, followed by finetuning the network using a low learning rate of 0.0005 and a batch size of 8. Random crops of 512×512 , color jittering, and random vertical and horizontal flips were performed of data augmentation. The Histology GCN and Genomic SNN were initialized using the self-normalizing weights from Klambour *et al.* [51], and trained with a learning rate of 0.002 with a batch size of 32 and 64 respectively. For the Genomic SNN, a mild \mathcal{L}_1 regularization was also used with hyperparameter value $3e-4$ to enforce feature sparsity. All networks were trained for 50 epochs using the Adam optimizer [57], dropout probability $p = 0.25$, and a linearly decaying learning rate scheduler.

After training the Histology CNN, for each 1024×1024 histology ROI, we extract $[32 \times 1]$ embeddings from 9 overlapping 512×512 patches, which we pair with their respective cell graph and genomic feature input as input into Pathomic Fusion. For the Histology GCN and Genomic SNN, we first trained their respective unimodal networks with the aforementioned training details, and then trained the last linear layers of the multimodal network with the unimodal network modules frozen with a learning rate of 0.0001 and Adam solver. At epoch 5, we unfroze the genomic and graph networks, and then trained the network for 25 more epochs using a learning rate of 0.0001, Adam solver, and a linearly decaying learning rate scheduler.

Evaluation Details

The predicted hazard and grade scores from each unimodal and multimodal network were evaluated on the test splits of the 15-fold cross-validation. To use the entire 1024×1024 histology image for CNN-based survival outcome prediction, similar to previous work, we computed the mean of hazard predictions from 9 overlapping 512×512 image crops across all histology ROIs belonging to each patient. For plotting the Kaplan-Meier curves, we pooled predicted hazards from all of the test splits in the 15-fold cross-validation and plotted them against their survival time. For creating the Swarm plots, we z-scored predicted hazards in each split before pooling so that scores for low vs. high risk would have similar ranges in visualization. On grade classification, since grade is determined solely from histopathological appearance, we did not ensemble classification scores.

APPENDIX C. ABLATION STUDIES AND COMPARATIVE ANALYSIS

TABLE II: Comparative analysis of the ensembling effects of unimodal networks. Overall, ensemble models of Histology CNN, Histology GCN, and Genomic SNN caused networks to overfit and decrease in performance. Improvements made by ensembling were marginal compared to improvements made by Pathomic Fusion.

Model	c-Index	<i>P</i> Value	AUC \uparrow	AP \uparrow	F1-Score (Micro) \uparrow	F1-Score (Grade IV)
Histology CNN	0.750 ± 0.010	$4.92\text{e-}17$	0.915 ± 0.007	0.852 ± 0.012	0.747 ± 0.013	0.901 ± 0.006
Histology (CNN + CNN)	0.749 ± 0.010	$1.40\text{e-}131$	0.920 ± 0.006	0.858 ± 0.011	0.756 ± 0.014	0.908 ± 0.007
Histology GCN	0.722 ± 0.014	$2.68\text{e-}12$	0.872 ± 0.009	0.793 ± 0.014	0.672 ± 0.017	0.861 ± 0.010
Histology (GCN + GCN)	0.720 ± 0.014	$3.96\text{e-}80$	0.880 ± 0.012	0.804 ± 0.019	0.688 ± 0.019	0.849 ± 0.015
Genomic SNN	0.808 ± 0.014	$8.92\text{e-}18$	0.872 ± 0.011	0.761 ± 0.018	0.670 ± 0.014	0.882 ± 0.015
Genomic (SNN + SNN)	0.794 ± 0.014	$2.522\text{e-}02$	0.869 ± 0.011	0.755 ± 0.020	0.668 ± 0.016	0.881 ± 0.016
<i>Pathomic Fusion</i> (GCN \otimes SNN)	0.812 ± 0.010	$3.86\text{e-}12$	0.913 ± 0.008	0.838 ± 0.014	0.742 ± 0.017	0.923 ± 0.010
<i>Pathomic Fusion</i> (CNN \otimes SNN)	0.820 ± 0.009	$2.39\text{e-}12$	0.925 ± 0.008	0.865 ± 0.014	0.754 ± 0.015	0.921 ± 0.008
<i>Pathomic Fusion</i> (CNN \otimes GCN \otimes SNN)	0.826 ± 0.009	$6.95\text{e-}13$	0.927 ± 0.009	0.866 ± 0.015	0.762 ± 0.018	0.932 ± 0.009

TABLE III: Number of trainable parameters for each unimodal and multimodal network used in survival prediction and grading. We demonstrate a $100\times$ reduction in the number of trainable parameters for GCN as compared CNN and a $13\times$ reduction in parameters when using Pathomic Fusion with GCN \otimes SNN as compared to CNN \otimes SNN.

Model	# Parameters (Survival)	# Parameters (Grading)
Histology CNN	26773569	26773635
Histology GCN	203588	203654
Genomic SNN	10961	11027
<i>Pathomic Fusion</i> (GCN \otimes SNN)	322114	307116
<i>Pathomic Fusion</i> (CNN \otimes SNN)	170130	103462
<i>Pathomic Fusion</i> (CNN \otimes GCN \otimes SNN)	1506054	898780

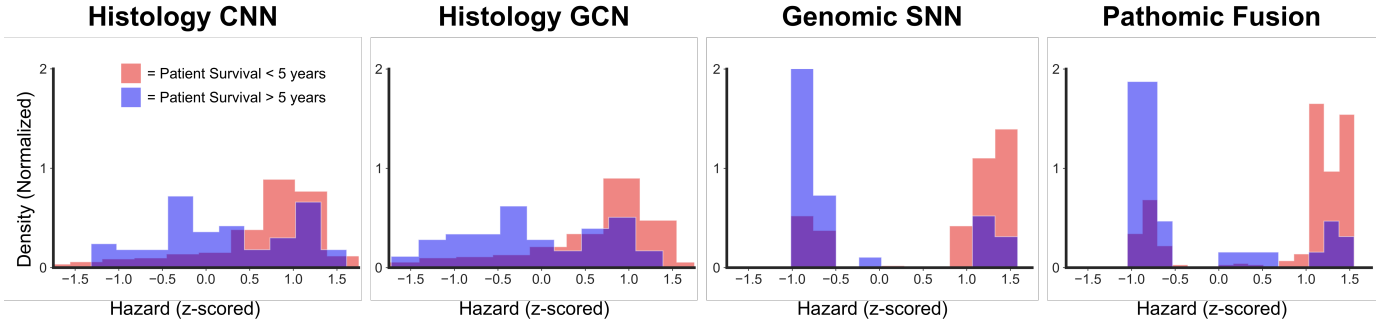


Fig. 7: Distribution of hazard [redictions for Histology CNN, Histology GCN, Genomic SNN, and Pathomic Fusion. Histology CNN and Histology had similar skewed distributions of hazard. Qualitatively, Genomic SNN produced 2 high density regions, while Pathomic Fusion produced 3 high density regions.

TABLE IV: Analysis that describes the admixture of grades and molecular subtypes in each high density region for Histology CNN, Histology GCN, Genomic SNN, and Pathomic Fusion. For Pathomic Fusion, the three high density regions corroborate with the WHO paradigm in separating gliomas into IDHwt ATCs, IDHmut ATCs, and ODGs. In patients with predicted hazard in $[-1.00, -0.50]$, we observe an admixture of Grade II and III gliomas, and IDHmut ATCs and ODGs (predominantly Grade II gliomas and ODGs). In the density region $[1.00, 1.25]$, we observe an admixture of Grade III and IV gliomas and IDHmut and IDHwt ATCs. In the density region $[1.25, 1.50]$, we observe mostly Grade IV gliomas and IDHwt ATCs. Pathomic Fusion was able to better assign Grade IV gliomas and IDHwt ATCs as high risk ($1.25 < \text{Hazard} < 1.50$) than Genomic SNN. The region $[-0.50, 0.00]$ was also predominantly Grade IV gliomas and IDHwt ATCs for Histology CNN and Histology GCN, which suggest that histology has less ability in assigning WHO Grade IVs as high risk.

Model	Density Region		Grade II (%)	Grade III (%)	Grade IV (%)		IDHwt ATC (%)	IDHmut ATC (%)	IDHwt ATC (%)
Histology CNN	$-0.50 < \text{Hazard} < 0.00$		8.38	20.78	69.57		6.37	9.65	60.19
	$0.50 < \text{Hazard} < 1.00$		1.80	10.27	87.93		2.16	4.86	75.32
	$1.00 < \text{Hazard} < 1.50$		2.25	6.98	90.32		0.68	5.41	70.50
Histology GCN	$-0.50 < \text{Hazard} < 0.00$		9.31	19.49	67.85		7.10	9.65	57.33
	$0.50 < \text{Hazard} < 1.00$		3.47	14.08	80.61		4.08	7.35	65.51
	$1.00 < \text{Hazard} < 1.50$		0.88	4.86	93.82		0.66	7.28	72.41
Genomic SNN	$-1.00 < \text{Hazard} < -0.50$		47.36	39.60	1.80		26.10	23.62	1.01
	$1.00 < \text{Hazard} < 1.25$		15.42	43.17	40.97		4.85	12.78	63.88
	$1.25 < \text{Hazard} < 1.50$		12.85	39.50	46.39		3.45	6.27	72.73
Pathomic Fusion	$-1.00 < \text{Hazard} < -0.50$		47.17	39.39	1.65		26.42	23.47	1.06
	$1.00 < \text{Hazard} < 1.25$		15.25	42.15	41.26		3.14	11.66	64.13
	$1.25 < \text{Hazard} < 1.50$		9.54	38.16	52.30		1.06	4.59	81.27

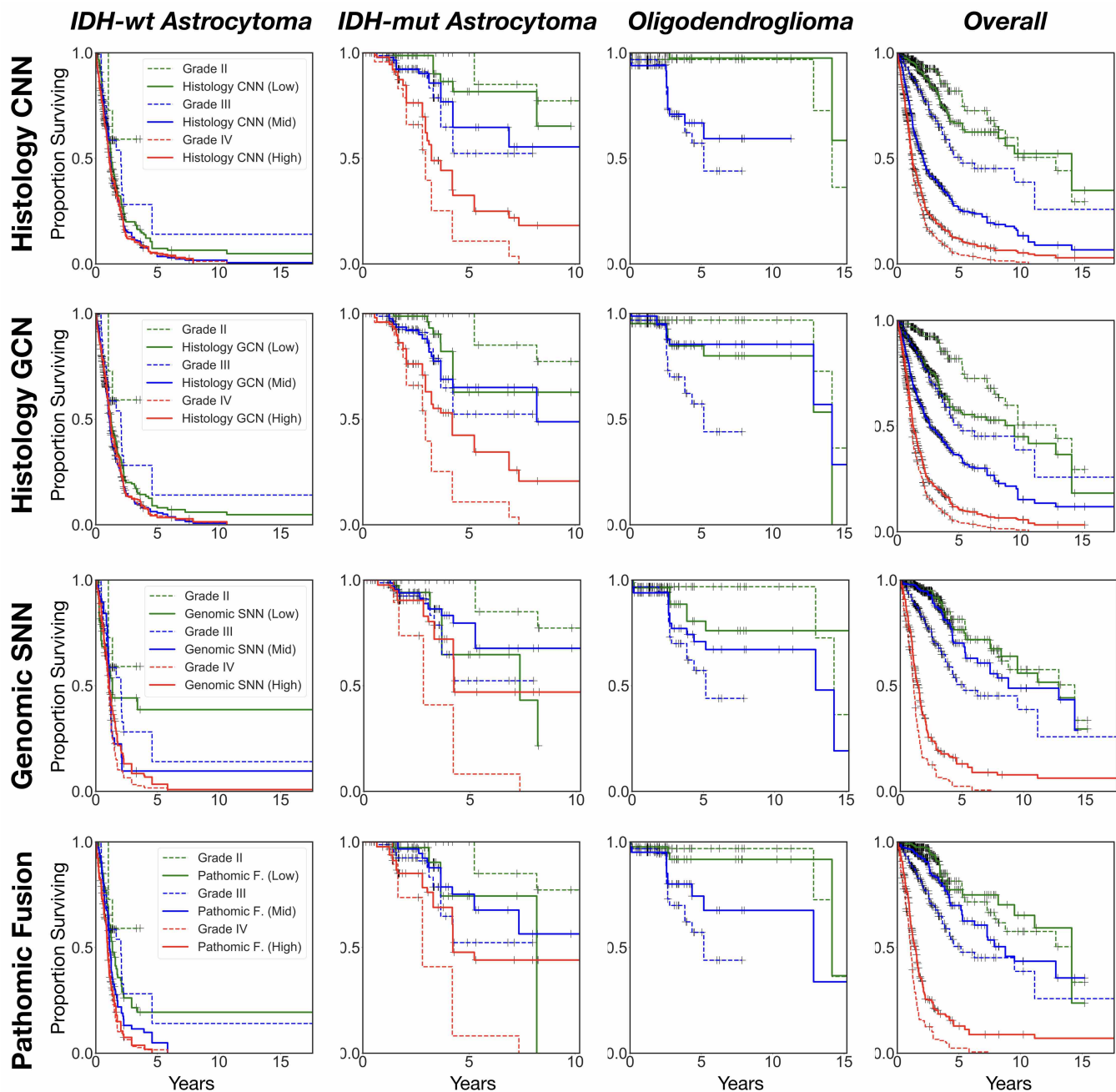


Fig. 8: Kaplan-Meier comparative analysis of Histology CNN, Histology GCN, Genomic SNN, and Pathomic Fusion with respect to IDHwt ATCs, IDHmut ATCs, ODGs, and all molecular subtypes in stratifying WHO Grades II, III, and IV using the 33-66 percentile of hazard predictions as a heuristic for separating patients into low/mid/high risk categories. Overall, we observe that this heuristic has similar stratification of patients as the WHO grading system.